Available online at www.sciencedirect.com
ScienceDirect
Robotics and Computer-Integrated Manufacturing 25 (2009) 155–167
Robotics and Computer-Integrated Manufacturing
www.elsevier.com/locate/rcim

Dimensional measurements of a gray-iron object using a robot and a laser displacement sensor

Jure Rejc*, Justin Činkelj, Marko Munih

Faculty of Electrical Engineering, University of Ljubljana, Tržaška 25, 1000 Ljubljana, Slovenia

Received 6 December 2006; received in revised form 24 October 2007; accepted 9 November 2007

Abstract

This paper presents a system for noncontact dimensional measurement of a gray-iron grate by use of a laser dot triangulation displacement sensor and an industrial SCARA robot. A special kernel driver and an associated dynamic link library were written for this system, enabling a higher sampling rate of the robot world coordinate positions and of the laser measurements. For repair of the scan data and calculation of the coordinates of deburring points, another program was written, where a unique approach of polynomial approximation to the profile was developed. To determine the accuracy of the robot measurement system, a number of comparative measurements were performed on a reference cube with a coordinate-measuring machine. Comparative measurements on real gray-iron grates were also done. The results show that dimensional measurements on a grate, at 88 points, can be performed within 45 s and with ±0.3 mm accuracy, which proved to be sufficient for robot deburring of gray-iron grates.

Keywords: Gray-iron deburring; Industrial robot; High-speed sampling; Laser triangulation; Noncontact robot dimensional measurement

1. Introduction

The work described here covers one part of the application of a robot for deburring gray-iron castings. The task is challenging owing to the very complex workpiece, called a grate or a mesh, which is used to carry pots on a cooking stove. Gray-iron grates, after cooling, have burrs of variable size. These must be removed to obtain a neat, smooth appearance. This paper describes the measurement robot system for a unique robot deburring approach based on a standard industrial robot carrying a stiff deburring tool. The ideal deburring trajectory, based on ideal CAD model, is adapted from dimensional measurements performed with a second robot in an earlier stage.

Foundries play an important role today in the manufacturing of various products around the world. This technology enables production of geometrically complex products in high quantity, leading to cheap castings. The process of casting, however, has a number of disadvantages. The most inconvenient are undesired projections of material, also called burrs. Burrs appear in the places where cast iron spills between the bottom and top of the casting mould or as a leftover of the gray-iron input flow channel. Burrs reduce the dimensional accuracy of parts, may complicate the subsequent assembly process, and also affect the appearance and geometry of the product. This means that all undesired material must be removed. Today, most frequently, the deburring task is done manually, accounting for up to 25% or even more of total production costs [1]. One of the biggest problems in the automation of burr removal appears to be the dimensional dispersion of castings, which is a consequence of irregular cooling conditions.

Many different approaches have been proposed in the past for automation of the deburring process. The following approaches are usually used for robotic deburring [2]: the compliant, the sensor-driven, and the force feedback approach. The first two methods are suitable for objects that do not need to be dimensionally precise. A few promising robotic laboratory experiments have been performed in the past, employing the force feedback

*Corresponding author. Tel.: +386 1 4768 379; fax: +386 1 4768 239.
E-mail address: jure.rejc@robo.fe.uni-lj.si (J. Rejc).
URL: http://robo.fe.uni-lj.si/staff-20.html (J. Rejc).

0736-5845/$ - see front matter © 2007 Elsevier Ltd. All rights reserved.
doi:10.1016/j.rcim.2007.11.001

deburring principle, mainly in the field of fuzzy control algorithms [3,4] for trajectory adaptation. Murphy et al. [5] proposed automatic generation of the trajectory of the robot based on a CAD model and force feedback for correction of the path of the robot.

The most important issue in this work, accurate dimensional or coordinate measurements, can be separated into two types [6]: contact and noncontact. Shen et al. [7] have classified coordinate-measuring machines (CMMs) with a touch-trigger probe sensor as contact solutions, while the noncontact solutions include laser scanners and vision systems based on video cameras. Sansoni et al. [8] have reported that noncontact sensors can be used in conjunction with CMMs to extend their capabilities, i.e. combinations of contact and noncontact measurement systems can be implemented.

The most accurate contact system is a CMM with a touch-trigger probe with an accuracy of under 1 μm, based on a serial or parallel mechanism. Better-performance CMMs are large and heavy, and therefore not capable of performing fast measurements [9]. Touch-trigger probes also slow down the measurements, because information is read one point at a time.

Frequently used noncontact measurement devices are laser distance sensors using a laser beam that can be projected onto a surface as a dot, a line, a group of parallel or perpendicular lines, or a circle. Common principle of operation of today's laser displacement sensors is based on the principle of optical triangulation [10], but it has some measurement limitations. More accurate measurement results are obtained by conoscopic holography. This is based on a simple implementation of a particular type of interference process of polarized light using crystal optics [11], which makes measurements possible where the triangulation principle fails. These two methods are suitable for very accurate measurements.

Video camera systems with three-dimensional (3D) coordinate acquisition are used in many applications. A typical example is the dimensional control of workpieces and the digitization of complex, free-form surfaces in reverse engineering. Two very important factors in camera vision systems are accuracy and field of view (FOV). The accuracy of the system needs to be sufficient to satisfy the purpose of the measurement, and the object needs to be within the FOV. Unfortunately, better accuracy can usually be obtained only with a smaller FOV. In addition, camera systems have other problems, including issues with lighting conditions and shadowing.

There are other aspects, linked to the shape and size of our workpieces, that need to be considered. To obtain satisfactory dimensional information for describing a whole grate, a minimum number of 88 points is needed. The desired measurement accuracy was set at ±0.2 mm in the work area, and the measurements were required to take less than 1 min for one workpiece. The number of points and the requirement on the time exclude methods based on contact principles.

A number of reasons prevented us from buying or developing a camera system: the unpredictable visible shape of burrs would make mathematical analysis very complex, the contrast of the object would be poor, and the large dimensions of the grate limit the measurement accuracy, even when using several cameras. In contrast, the measurement principle of triangulation using a laser dot sensor has a high resolution, in the range of micrometers, and could enable fast acquisition of neighboring points and shapes.

The laser sensor may be fixed and the scanned part moved, or the laser sensor may be moved; nowadays, this is done mostly by use of ordinary industrial robots [12]. The approach of moving the laser has many advantages, allowing flexible, programmable systems, and also small stand-off distances. Homh et al. [13] state that the main drawbacks of these systems are problems of long-term stability, vibration as a consequence of high accelerations and decelerations, the impact of temperature variations on the robot, and a very high price.

In the work described in this article, we have taken the pool of published knowledge, utilized high-accuracy sensors and a moving robot, developed specific software for accurate acquisition, and performed shape modeling of the grate in order to increase the accuracy and robustness. To check the validity of the measuring method, 42 grates were measured first using this technology and then checked with a calibrated CMM. The results are provided, with a basic statistical analysis, along with a discussion and final conclusions.

2. Hardware

The system that we used for dimensional measurements of grates is shown in Fig. 1. It is made by combining an Epson industrial robot used for carrying a Micro-Epsilon laser dot triangulation sensor with an A/D converter for acquisition of the analog output signal from the laser, and a table to which the grate was fastened.

2.1. Epson E2S651 robot

The SCARA (Selective Compliant Assembly Robot Arm) Epson E2S651 robot with 4 DOF (degrees of freedom; RRTR—rotation, rotation, translation, rotation) is mainly used for automation of assembly in industrial processes. It has a cylindrical working range from 280 to 650 mm. The repeatability specifications are very good: 15 μm for the first and second axes, 10 μm for Z-axis and 0.02° for U-axis.

The Epson robot was used as an X and Y world coordinate measurement tool, and as a carrier for the laser dot distance sensor for acquisition of the Z coordinate. This application required a higher sampling frequency from the robot than was possible with standard software. For this purpose, a kinematic model for the first and second axes was needed (Eqs. (1) and (2)). The value of the

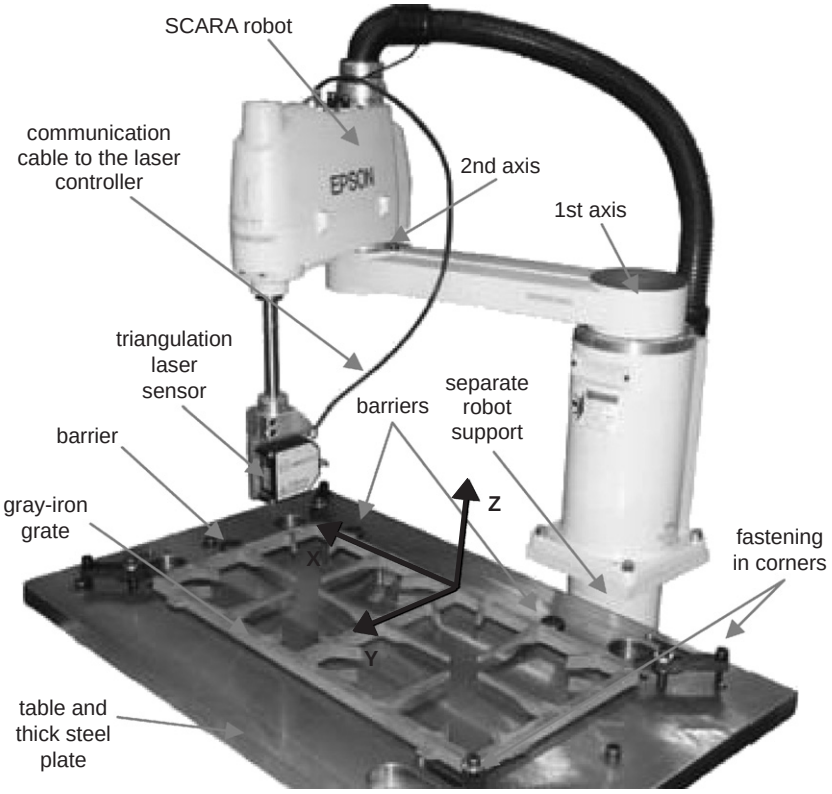

Fig. 1. Measuring system, table and gray-iron grate.

constant d_1, as a length of the first robot segment, was 415 mm and that of d_2, as a length of the second robot segment, was 235 mm. The variable ϑ_1 stands for the angle of the first axis and ϑ_2 for that of the second axis.

$$X = d_1 \cdot \cos\vartheta_1 + d_2 \cdot \cos(\vartheta_1 + \vartheta_2), \quad (1)$$

$$Y = d_1 \cdot \sin\vartheta_1 + d_2 \cdot \sin(\vartheta_1 + \vartheta_2). \quad (2)$$

The relationships between the encoder reading (N_1) for the encoder value at joint 1 and N_2 for the encoder value at joint 2, and the joint angles in the following equation are

$$\vartheta_1(^\circ) = \tfrac{1}{910.2} \cdot N_1, \quad \vartheta_2(^\circ) = \tfrac{1}{568.9} \cdot N_2. \quad (3)$$

The robot controller of type RC420 was based on an industrial PC platform with Microsoft Windows 2000 Professional operating system.

2.2. Laser triangulation distance sensor

For the noncontact measurement of the vertical coordinate, a Micro-Epsilon ILD2200-10 laser dot triangulation system was used. This combined a laser head with a laser beam source, a CCD camera and an appropriate controller. The measurement range of this laser system was 10 mm, the stand-off or reference distance was 35 mm from the laser head, the resolution was 0.5 μm, and the linearity was ±0.03% of full-scale output. The beam size at the middle of the measurement range was 50 μm, and at the edge of the measurement range 110 μm. All of these data apply to a diffusely reflecting matt white ceramic surface. In the present system, the analog voltage output of ±5 V was used. The controller also had two special digital-output status pins: POOR TARGET indicated that the object was not in the measurement range, and OUT OF RANGE that the object was at the edge of the measurement range. Both of these signals were exploited in the present measurement system.

2.3. Analog-to-digital converter

In the system, the analog voltage output from the laser controller was converted by an analog-to-digital converter, connected directly to the LPT port of the industrial PC platform of the Epson robot. The free pins of the parallel cable connected the two additional special signals from the laser sensor (left side of Fig. 2). The analog-to-digital converter was of type MAX197BCNI, 12-bit, a 6 μs conversion time and a 100 ksps sampling rate.

2.4. Robot and grate fastenings

The robot was fixed 870 mm from the floor on a massive vertical circular tube, which was then fixed to a heavy concrete pedestal lying on the floor. The world coordinate system of the robot and the work table were set as parallel as possible and were not connected, to avoid transfer of

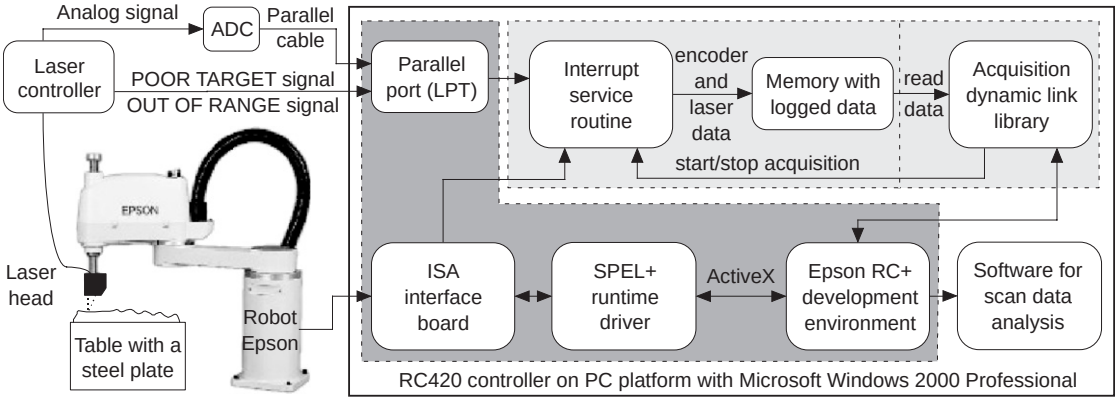

Fig. 2. Connection scheme and operating principle of the Epson robot measuring cell.

vibrations. On the top of 650 mm wide, 850 mm high, and 600 mm long work table was placed a special heavy steel plate, which could be leveled vertically by three screws to set a horizontal plane parallel to the horizontal moving plane of motion of the Epson robot. The steel plate was 800 mm wide, 30 mm thick, and 480 mm long. On the top of the plate, three circular barriers were fixed, meant for positioning a grate parallel to the world coordinate axes of the robot. This steel plate also had four clamps for fastening the grate and preventing any movement during laser scanning. The test grate was approximately 265 mm wide, 20 mm high, and 550 mm long. Gray-iron material was an alloy of carbon (3–4%) and iron (97–96%); the grain size of the mold was 0.2 mm.

3. Software

3.1. User environment

To increase the positional sampling rate of the robot, to enable faster scanning, from 100 to 500 Hz, custom-designed software was used. The Epson RC+ development environment uses Windows and a variant of the BASIC language. The environment can call the standard Epson robot functions, as well as new functions implemented in external dynamic link libraries (DLLs).

The programs written in BASIC communicate with a SPEL+ runtime driver using ActiveX technology. The SPEL+ runtime driver communicates with an ISA interface board, containing its own processor for real-time control of the power amplifiers and for passing the positional information to the circuits operating with the interface (dark gray area in Fig. 2).

For dimensional measurements using a robot and laser, a high, constant sampling rate of the position coordinates of the robot and of the analog output of the laser is needed. The Windows-based operating system and its associated software enabled sampling frequencies of only up to 100 Hz and the inter-interval time was not constant. A new dedicated driver and DLL functions were needed to overcome these shortcomings.

3.2. Robot encoder and laser data acquisition software

The new robot software was written in the Microsoft Visual Studio 6.0 development environment utilizing the C/C++ programming language. It has two sections: first, an interrupt service routine and memory for temporary data storage, which were part of a driver in the kernel space, and second, an acquisition DLL that was part of the user space, enabling control over the driver in the kernel space (Fig. 2, light gray area).

The registers of the ISA interface board for containing the encoder positions were not updated instantly, but at a rate of 500 Hz, with a counter indicating the changes of the values of the registers. The new software (the interrupt service routine) synchronized the reading of encoder positions by connecting to a synchronous interrupt that was triggered by the ISA interface board. The starting and stopping of triggering were supervised by appropriate functions from the acquisition DLL. Tests showed that the interrupt ran at a frequency slightly faster than 1 kHz. This meant that the interrupt was not called exactly twice as fast as the encoder position registers were updated. For this reason, the age of the encoder position data of the robot could be anywhere between 0 and 1 ms, meaning that the system was multirate [14]. Apart from reading the encoder registers, the interrupt service routine also reads the value of the laser triangulation sensor, via the parallel port.

The interrupt service routine log included changes of the encoder position, the values of the ISA register counter and the laser data, all saved into memory at the rate of the ISA interrupt. These data could be read from memory into the user development space by the acquisition DLL function, but only after the interrupt service routine was stopped. Before writing the data into a text file with a .scn extension, the encoder changes were converted into X and Y coordinate positions by the kinematic model of the robot, described by Eqs. (1) and (2).

3.3. Laser scanning errors and laser data analysis software

The software for analysis of the robotic laser measurement was developed especially for dimensional scanning of grates. It was written in the Borland Builder C++ 6.0 development environment. Scanning of the grate was performed first in the X direction of the robot world coordinate frame and then in the Y direction. During scanning, most of the path, in between the bars of the grate, does not belong to the object area. In these regions the speed of movement can be high, in contrast to other areas, where the full accuracy is needed. For this reason, a reduction of the speed of movement was needed to avoid having too large distance between two samples, which would be dependent on the sample acquisition rate and the speed of movement of the robot.

An algorithm that summarizes the processing of positional and laser data is shown in Fig. 3. It starts with user-defined input parameters (Level I) and the reading of .pnt file (Level II) for the movement trajectory of the Epson robot in the area surrounding where the object is lying. With this information, a corresponding path sequence is extracted from a .scn file (Level III) and further analyzed.

During laser scanning, errors can occur, and this erroneous data must be repaired or program execution must be stopped (Level IV). In our case, errors such as holes in the profile and outliers occurred. A hole phenomenon can be seen on the right-hand side of the profile in Fig. 4, where the horizontal axis displays the horizontal X coordinate of the robot and the vertical axis shows the laser distance readings. Teutsch et al. [15] mentioned that a very common error in laser scanning is caused by a shadowing effect, when the path of the laser beam is broken by an obstacle. In our case, shadowing was avoided by an appropriate orientation of the laser during scanning. The program repaired holes and outliers by ordinary linear interpolation if fewer than five points were erroneous.

The measurement range of 10 mm also allowed burrs to be seen in some scanned areas. Burrs are not part of the end product, and therefore burr data was removed from further analysis (Level V). To be able to set the boundaries for removing the burr data, an additional file with a .dis extension was included. This file was manually filled with distances from the top of a burr to the top of a bar of the grate for every scanned point. Using this information, the scan points representing burrs could be excluded from further analysis.

In the following step, deburring coordinates had to be set or calculated. In the majority of scanned profiles, the burrs were not visible or data on the burrs had been removed, meaning that a method for obtaining a mathematical approximation to the missing data was needed (Level VI). To approximate the slope of the grate, a polynomial function of degree n, where n was equal to 4, 6, and 8 (Eq. (4)), was used. In the polynomial equation (4), p stands for the polynomial coefficients, x is the horizontal

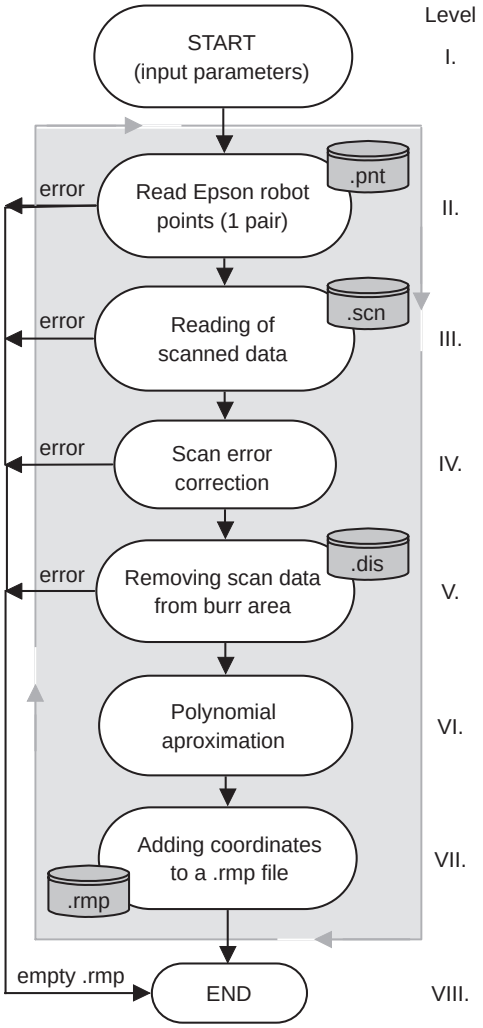

Fig. 3. Algorithm of laser scan and data analysis software.

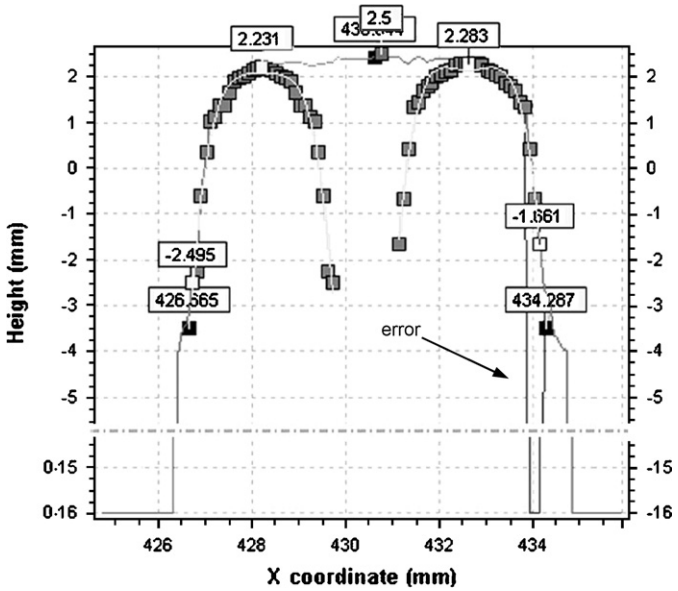

Fig. 4. Grate profile, scanning error, and polynomial approximation.

robot coordinate, and $\hat{y}$ is the calculated vertical value. With single polynomial one sloping side could be approximated, so two polynomials were needed to cover left-hand and right-hand slopes of the profile. Number of scan points used for polynomial approximation was also changeable, meaning that the width of the dish-shaped series of points could be increased or decreased. This procedure gave a variable width dish-shaped series of points, which can be clearly seen in Fig. 4, for both the left and the right approximation areas. Using a least-squares method (Eqs. (5) and (6)) and this dish-shaped data, all polynomial coefficients were calculated for each measured column of the grate

$$\hat{y} = p_0 + p_1 \cdot x + p_2 \cdot x^2 + \cdots + p_n \cdot x^n, \tag{4}$$

$$A = [1, x, x^2, \ldots, x^n], \tag{5}$$

$$p = [A^{\mathrm{T}} \cdot A]^{-1} \cdot A^{\mathrm{T}} \cdot y. \tag{6}$$

The approximation procedure was started with a polynomial of degree 4. The calculated mathematical approximation was compared with the laser measurements by using the residuals and the factor R^2, called the coefficient of determination. This coefficient had a value between 0 and 1.

$$ResidualSS = \sum (y - \hat{y})^2,$$

$$TotalSS = \sum (y - \bar{y})^2,$$

$$R^2 = 1 - \frac{ResidualSS}{TotalSS}. \tag{7}$$

R^2 was calculated using Eq. (7), where y is the value measured with the laser, $\bar{y}$ is the mean of the measured values, and $\hat{y}$ is the calculated value at a certain horizontal robot coordinate. If R^2 was greater than or equal to a value specified as an input parameter of the program, then the current degree of the polynomial was used. In other cases, the degree of the polynomial was increased by 2 and the calculation was repeated. In cases when even the higher polynomial failed, the width of the dish-shaped series of points was changed and approximation with an use of the polynomial with degree 4 was started again. If all variations failed the last measured point from the left and right parts of the profile was used for deburring. This method could be used universally for estimating the dimensions of objects of other shapes. The dimensional measurements of a cube that are presented later in this article exploited the same principle, only that the polynomial approximation always failed and uses only the laser scan points.

The algorithm in Fig. 3 was performed over all scan areas of the object. All points of the deburring profile were then saved into a .rmp file (Level VII). In the case of an error during analysis, the .rmp file had a length of 0 bytes (Level VIII).

4. Measurement methodology

4.1. Dimensional measurements of the calibration object

To check the measurement accuracy of the robot equipped with the laser, a reference object in the form of a perpendicular cube with known, verified dimensions was used. The dimensions of the cube were acquired between measured points on its surface, as can be seen in Fig. 5. To get the most accurate reference point coordinates, a CMM was used, periodically maintained and calibrated to fulfill the ISO 10360-2 standard [16]. The CMM had a planar length-measuring performance of $U2 = 3 + 4 \cdot L/1000$ (L is length of the measured object) in units of micrometers, and a volumetric repeatability of $R3 = 4\,\mu m$. The measurements were performed at a temperature of 20.6 °C with a touch-trigger probe of diameter 2 mm. The cube coordinate system for reference measurements was fixed by touching two perpendicular sides of the cube at a few points. The coordinate system through these points was set automatically by the CMM software. The subsequent measurements of all points, repeated 10 times, were also automated.

The reference object was approximately 50.3 mm wide, 51.2 mm high, and 64.7 mm long, made out of steel with a hardness of 249 HV (Vickers Hardness), with sharp edges, and ground and sanded surfaces. The high reflectivity for the laser beam was reduced by surface sanding. Additionally, one side of the cube was painted with black matte black paint and measured using the same methodology. The reason for painting one side of the cube was work by El-Hakim et al. [17], where laser measurement errors were presented for cases where sudden changes in surface height occur, large variations in the reflectance or color of the surface exist, or the surface is rough.

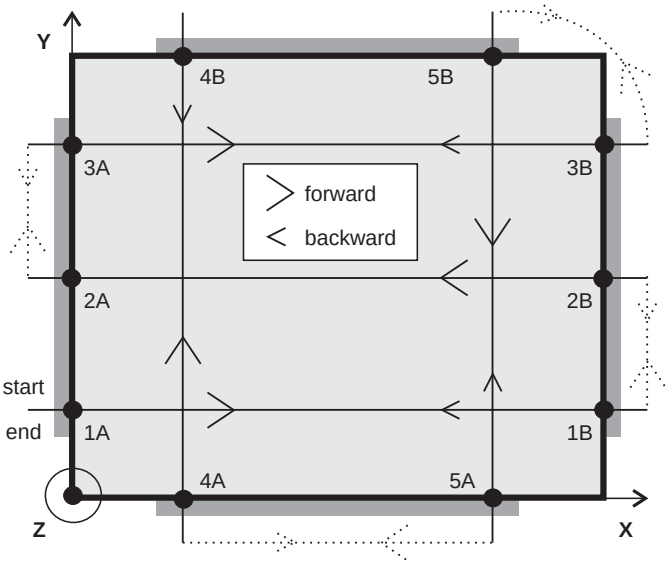

Fig. 5. Reference cube, rubber strip, and scanning trajectory.

During the robot measurements, the test cube was laid on the top of a heavy steel plate, previously leveled according to the plane of motion of the robot. The cube was placed in nine (3×3) positions in the robot work area, filling most of the cylindrical working range. Robot measurements were performed at different measurement speeds; the scanning speeds were 10, 20, 50, and 100 mm/s. At a sampling rate of 500 Hz this represents horizontal linear resolutions of 0.02, 0.04, 0.1, and 0.2 mm.

Five scanning lines were drawn on the cube, three in the X direction and two in the Y direction of the coordinate system of the cube (Fig. 5). Each of the scan cycles included moving the laser first in the forward and then in the backward direction. In all paths, the laser head was oriented in the same way relative to the direction of progression in order to prevent shadowing effect. The number of repetitions of the scan was 30 in both directions; each direction is marked in Fig. 5 by larger and smaller arrows. The top surface of the cube was placed in the middle of the measurement range of the laser, where the spot size of the laser beam was smallest. The environmental temperature during the measurements was 22 °C.

The first batch of measurements was on the unpainted side, followed by the painted side. On the painted side, a black rubber strip was also attached, 6 mm from the top and 3 mm in width, shown in Fig. 5 as a dark gray area. This prevented enlargement of the laser beam diameter if the measured surface was more than 2 mm out of the laser range. The reason for attaching the strip only to the painted side originated from the grate surface, which was nearly black and not completely vertical at the edges.

The scan data from the test cube was analyzed using the same software as applied for analysis of the scanning of grates to give edge point coordinates.

4.2. Dimensional measurements of gray-iron grates with CMM and robot

The most realistic test objects were gray-iron grates themselves, dimensionally checked with the same CMM as described in the case of the cube measurements. The other measurement conditions and other equipment were also the same. The grates used in the measurements with the CMM and, later, with the robot system were not the same, owing to the measurement and deburring sequence, preventing an exact direct comparison. A statistical dimensional analysis will be shown instead.

The CMM coordinate origin was set at the middle of the grate by touching the outside edges at several points. The CMM program scanned 30 grates by touching 88 points, 40 in the X direction, and 48 in the Y direction on every grate. To equalize the conditions and avoid burrs, all points were touched 1 mm above the position of burrs. The total time consumed for one grate was approximately 7 min.

Forty-two grates were measured using the robot and laser measurement system. Each grate was positioned into the robot workspace, laid on the leveled steel plate and pushed to the three circular barriers (Fig. 1), so that it was parallel to the robot world coordinate system. Forty-four areas were scanned, 20 in the X direction and 24 in the Y direction, as can be seen in Fig. 6, marked with thick short lines. The scanning path was set as near to the CMM points as possible. The speed of the laser head was 50 mm/s inside the scan area of the grate (thick short line) and 500 mm/s otherwise. The distance between the laser head and the top of the grate was 31 mm, having 9 mm of measuring range of the laser available. The total time required for measurement of all 88 points was approximately 45 s. The deburring coordinates were later calculated using custom software for analysis of the scans.

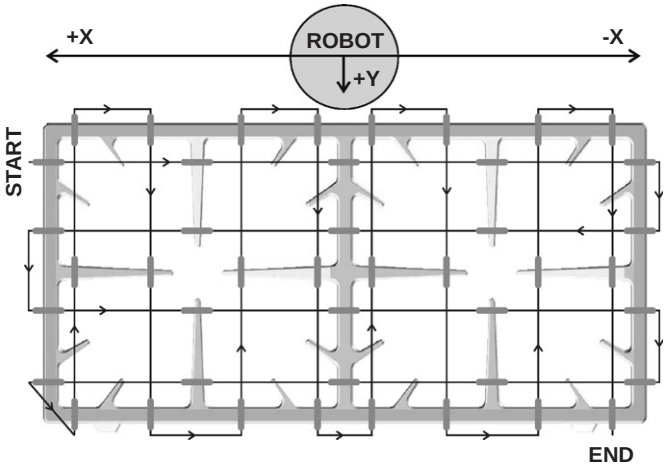

Fig. 6. Robot scanning path for gray-iron grate.

5. Robot measurement results

5.1. Dimensional measurements of the calibration object

Fig. 7 shows the dimensional error between the CMM measurements and the laser measurements for a speed of movement of the laser 20 mm/s. The results are for two different positions in the working range of the robot, marked as 5 and 4. The top two charts are for the unpainted surface, and the bottom two for the black-painted cube surface. In position 5, the scanning direction was from 4A to 4B, while in position 4, the direction was from 3B to 3A (Fig. 5). The horizontal axis represents the measurement number and the vertical axis the dimensional error in millimeters. If the CMM dimension is larger than the dimension measured with the robot laser system then the result is negative.

The charts for the unpainted surface (top two) show maximal dimensional errors of 0.13 and 0.26 mm, with mean errors of 0.08 and 0.19 mm. In other cube positions in the robot work area, both smaller and larger dimensional differences occurred, from −0.06 to 0.30 mm. The maximal errors for the painted surface, shown in the bottom two charts, are −0.12 and 0.13 mm, with mean values of −0.07

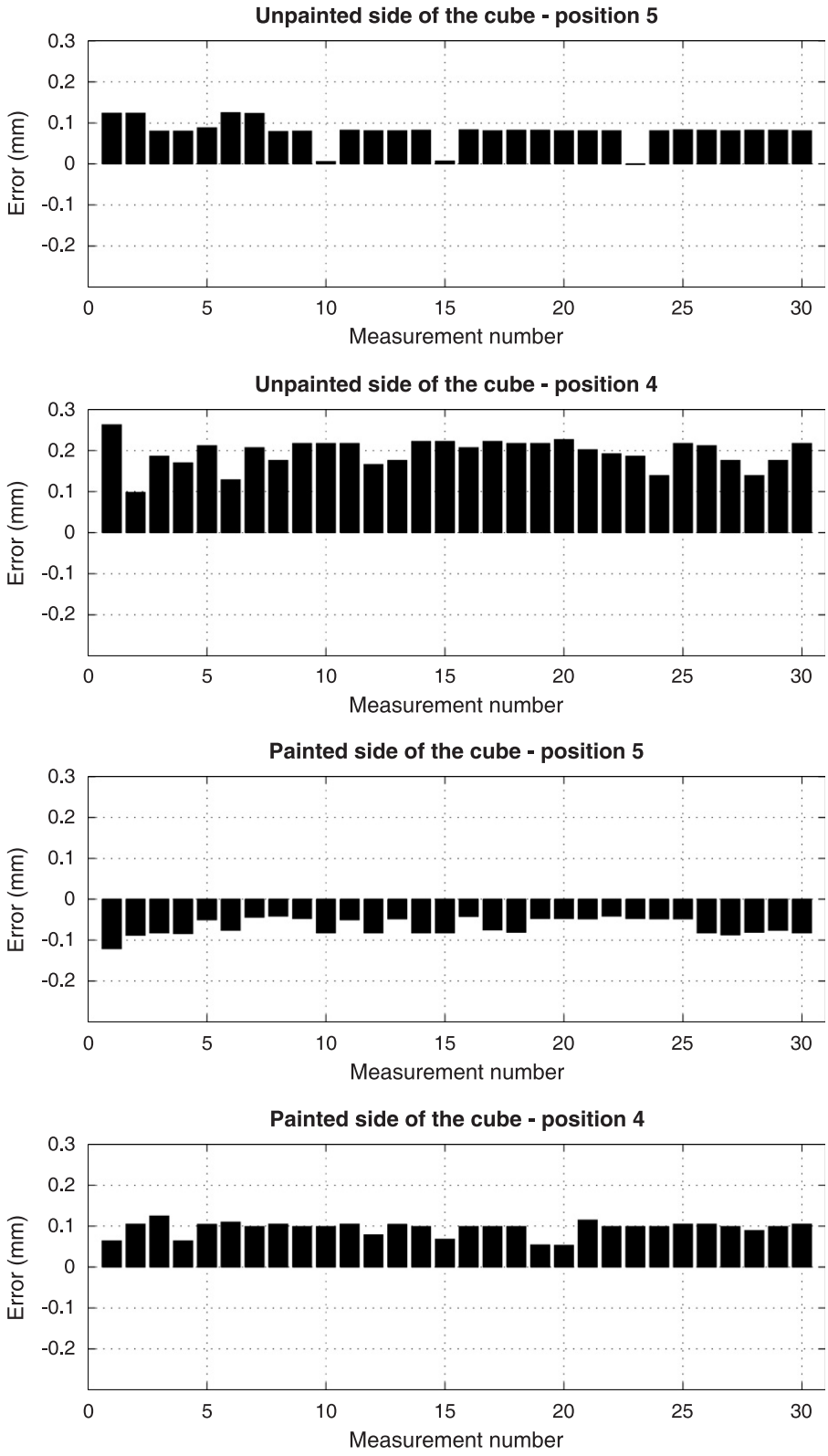

Fig. 7. Error between laser and CMM measurements at scanning speed of 20 mm/s.

and 0.09 mm. In other cube positions within the robot working area, the dimensions varied from −0.17 to 0.15 mm.

Fig. 8 also shows the error, as calculated, between the CMM and laser measurements, when the speed of movement of the laser head was set to 50 mm/s, the same as when the grates were inspected dimensionally before deburring. The top two charts show results for the unpainted surface, and the bottom two charts for the

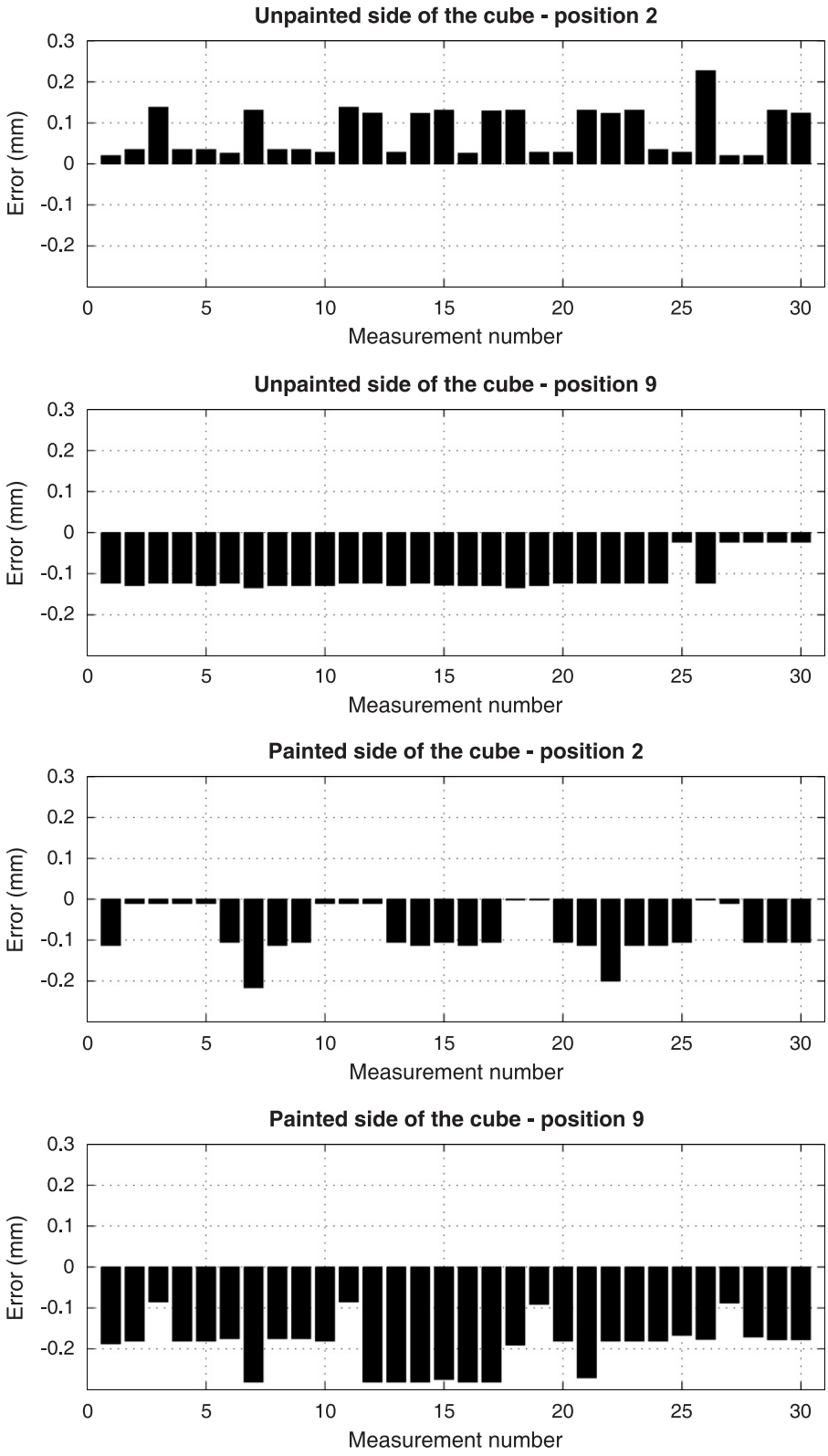

Fig. 8. Error between laser and CMM measurements at scanning speed of 50 mm/s.

painted surface. In position 2, the scanning direction was from 2A to 2B, while in position 9, the direction was from 4B to 4A. The horizontal axis represents the measurement number and the vertical axis displays the dimensional error in millimeters, where a positive value stands for the case when the real cube (as measured with the CMM) was larger than the result of measurement by the robot laser system.

An immediate comparison between Figs. 7 and 8 shows larger measurement errors when a higher scanning speed was used. For the unpainted surface, the top two charts show maximal errors of 0.23 and −0.13 mm, but the mean error differs only slightly from the results at lower speeds. The mean values are 0.08 mm and −0.11 mm. In other cube positions in the robot work area, the results show dimensional errors between −0.17 and 0.31 mm. For the painted surface, the bottom charts show maximal errors of −0.22 and −0.28 mm, with mean values of −0.08 and −0.19 mm. The whole series of measurements show that the error on the painted surface can be from −0.30 to 0.13 mm. The minimal and maximal error results for all end-effector speeds tested and for both cube surfaces are shown in Table 1.

5.2. Dimensional measurements of gray-iron grates with CMM and robot

The chart in Fig. 9 shows the standard deviation over 30 grate samples for each of the 88 points measured with the CMM. The horizontal axis represents the number of the measured point on the grate and the vertical axis shows the standard deviation for all measured points in millimeters. The first observation is that the real grates differ dimensionally. The mean standard deviation for all 88 points on 30 grates is 0.13 mm, and the maximal standard deviation is 0.31 mm. The maximal error at one point was larger than the statistically calculated value and was determined to be 1.47 mm. A few areas of the grate where larger errors occurred can be clearly seen in Fig. 9. Positions on the grate showing such errors are expected, since these areas of the grate have one of their ends free and can be more easily bent in the process of cooling. These results also confirmed the necessity to measure all grates prior to their deburring.

Table 1
Extreme error values between CMM and robot laser measurements

Cube surface	Unpainted		Painted	
Scanning speed (mm/s)	Error (mm)		Error (mm)	
	min	max	min	max
10	−0.01	0.33	−0.16	0.19
20	−0.06	0.30	−0.17	0.15
50	−0.17	0.31	−0.30	0.13
100	−0.31	0.29	−0.54	0.12

The bars in Fig. 10 show the normalized error of all measurement points according to a mean point value, quantized in steps of 0.05 mm. The solid line represents the ideal Gaussian distribution for the current data. The measured data fit very well to the ideal Gaussian distribution. On the right-hand side of the figure, however, a few outliers occur, and these can cause serious problems in the robotic deburring process.

A similar analysis was performed on data obtained using the robot and laser noncontact measurement system. Fig. 11 shows the standard deviation for 88 points on 42 grates. The horizontal axis represents the number of the measured point, and the vertical axis the standard deviation for all measured points in millimeters. The common standard deviation is 0.17 mm, a little larger than that in the CMM measurements. The maximal standard deviation is 0.32 mm, and the maximal deviation at one point is 1.91 mm. As can be seen in Figs. 9 and 11, the

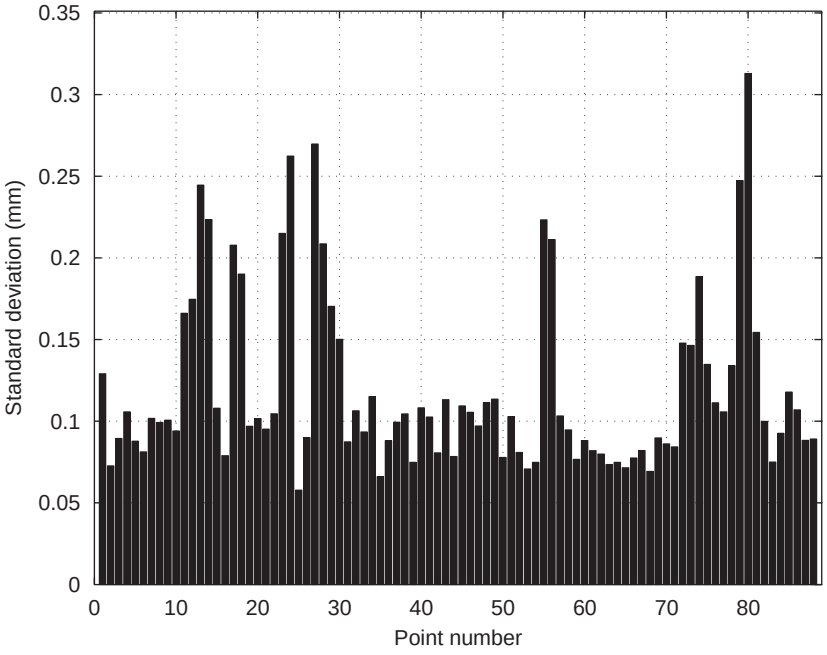

Fig. 9. Standard deviation with CMM measured coordinates of 88 grate points.

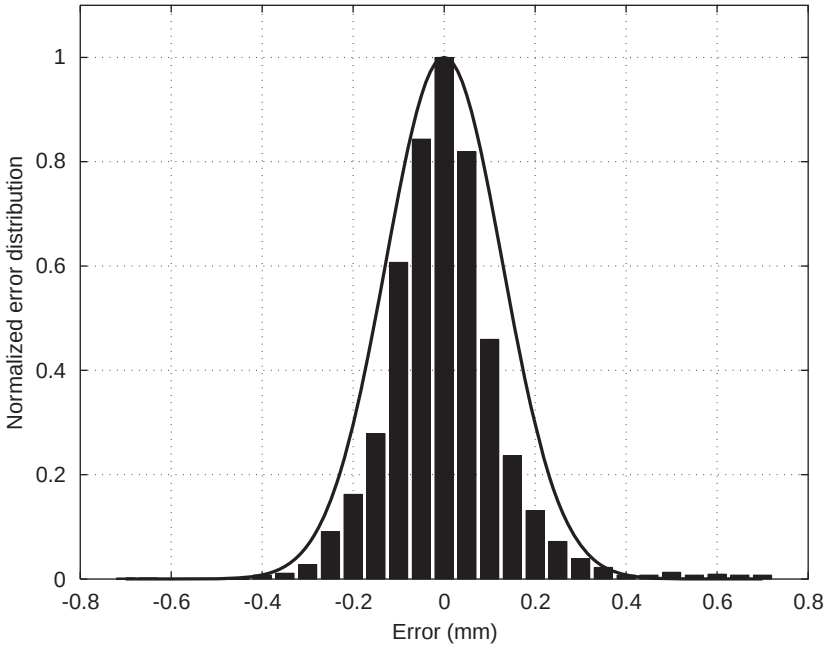

Fig. 10. Ideal Gaussian distribution and distribution with CMM measured grate points.

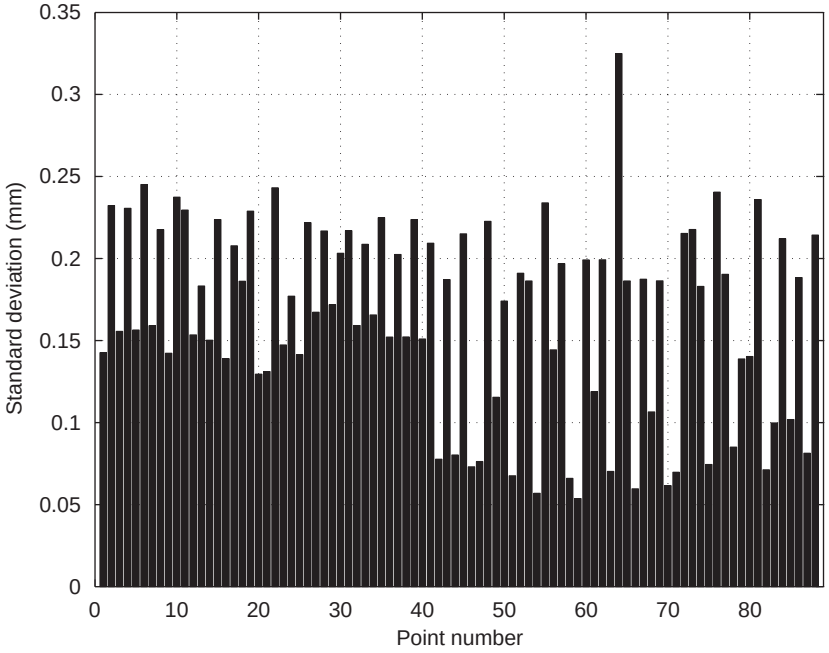

Fig. 11. Standard deviation with robot and laser measured coordinates of 88 grate points.

differences between the results for the CMM and the system described here are small. This confirms the suitability of the dimensional measurements of the grates made with the robot and the laser.

The distribution of grate dimensions measured with the robot can be seen, as bars in Fig. 12. The solid line represents the ideal Gaussian distribution. When one compares the bars and the solid line agreement can be noted with a few examples of more deviation in the values at the edges.

6. Discussion

From the measurement results acquired from the reference cube, it can be concluded that the dimensional error between the contact approach and the approach

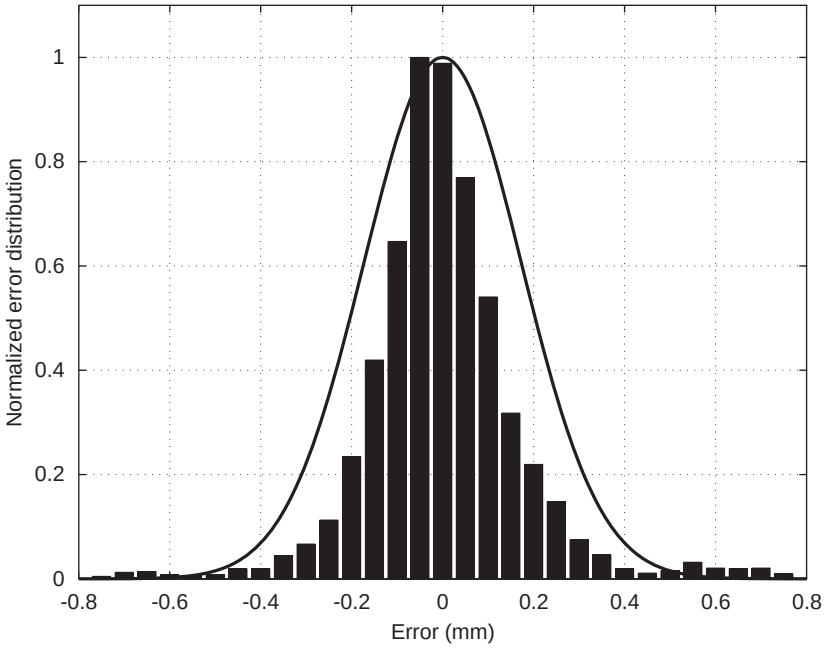

Fig. 12. Ideal Gaussian distribution and distribution with robot and laser measured grate points.

using a robot with a laser (Figs. 7 and 8) is higher than expected. One source of the error is the sampling frequency of the robot encoder, set at 500 Hz. This gives a coordinate resolution of 0.04 mm at an end-effector speed of 20 mm/s and 0.1 mm at an end-effector speed of 50 mm/s. As mentioned before, the sampling of the encoder does not give a constant sampling rate, but instead the sampling time varies between 0 and 1 ms, which causes the object dimensions to be shorter by twice the position resolution. At a robot end-effector speed of 50 mm/s, this causes a dimensional reduction of −0.2 mm.

The errors in laser measurement are important. Curless et al. [18] have described how, in optical triangulation systems, the accuracy of the range data depends on the proper interpretation of the light reflections imaged. Sensors based on the triangulation principle can give irregular measurements if the laser beam hits the edge of the object or if a reflectance discontinuity is present on the surface of the object.

The majority of the measurements in this study showed that the dimensional differences between the CMM and the robot measuring system were smaller on the black-painted surface, which was also equipped with a black rubber edge. This confirms the statement about enlargement of the laser beam when it hits a surface more than 2 mm out of the measurement range of the laser.

Also, the choice of a reference object with a high-reflectance surface and sharp edges was suboptimal. A better choice would be an object with slightly rounded edges and surfaces painted with a matte black coating, similar to the case of grate edges. But even with these improvements, it has been reported that triangulation sensors may return false measurement results. Häusler et al. [19] learned from experiments that laser illumination is not the best choice for triangulation. As stated there, coherent noise is the major source of measurement uncertainty in triangulation on rough surfaces.

Kinematic equations (Eqs. (1) and (2)) were used for calculation of the robot world coordinates. In the case of poor matching of these equations to the right parameters, the dimensional errors could be significant. That is why a series of measurements were performed beforehand. The motion coordinates of the robot acquired via kinematics in the world coordinate system were compared with readings from a micrometer with 1 μm resolution and 25 mm working range. Additional tests were performed by using an OPTOTRAK noncontact 3D positioning system. This had a 0.01 mm 3D resolution, an X and Y accuracy of 0.1 mm and a Z accuracy of 0.15 mm. The measurement range of these tests was 1140 mm with an end-effector speed of 50 mm/s. The results showed that the differences were within the range of the robot parameters, were initially known and could not be prevented. This means that the kinematic equations did not contribute significantly to the measurement error.

The dimensional results on real grates (Figs. 11 and 12) show noticeable dimensional differences among the grate samples. This suggests that one deburring trajectory will not fit several grates. More detailed verification of the CMM and robot measurement results, based on graphs for numerous points, which we have omitted from this paper for reasons of space, confirmed even more strongly that there was nonlinear shrinkage in both of the observed coordinates. For deburring purposes, the robot trajectory must be adapted to fit the measured coordinate values of the current grate. Comparison between the results of measurements made with the CMM and those made with the robot and laser shows that when the polynomial

approximation is used, the robot and laser system works very well, giving same class of accuracy for both measurement methods. This was the case when there were no sharp edges on the grates.

At the beginning of study, two requirements were specified. The first targeted the total time needed for completion of the dimensional measurements of one grate at 88 points. The target was set at 60 s, whereas the task was performed in 45 s. The second requirement targeted the measurement accuracy, with the hypothetical benchmark set at ± 0.2 mm. Unfortunately, this requirement was not reached completely, but we managed to be accurate to ± 0.3 mm.

In the final step, in a real deburring operation with a larger robot, 93 grates were very successfully cleaned completely. A robot complemented with a laser measuring system is now serving as a measuring device in a process for deburring of gray-iron grates. All this is also thanks to adaptive-order polynomial fitting, which increases the accuracy of the measurements and the robustness of the coordinate determination.

7. Conclusions

A system for noncontact dimensional measurement of gray-iron grates using a laser and an industrial robot has been developed. The original sampling rate of the robot was increased from 100 to 500 Hz for the robot world coordinates and the laser distance measurement signal. This enabled higher speeds of movement of the robot and laser without loss of coordinate resolution. The accuracy and robustness of the coordinate acquisition were assured by fitting the slope of the grate by a polynomial.

In comparison with the ultimate CMM approach, this noncontact system is faster, but less accurate. The system might be also well used for dimensional inspection of other objects, for inspection of the mounting of parts of assemblies, and for other types of industrial control of part dimensions.

Acknowledgment

This work was financially supported by ETA Cerkno factory.

References

[1] Chang SF, Bone G-M. Burr size reduction in drilling by ultrasonic assistance. Robotics Comput-Integrated Manuf 2005;21:442–50.

[2] Gillspie LK. Deburring and edge finishing handbook. Society of Manufacturing Engineers. New York: American Society of Mechanical Engineers, Corp; 1999.

[3] Hsu FY, Fu LC. Intelligent robot deburring using adaptive fuzzy hybrid position/force control. IEEE Trans Robotics Autom 2000; 16:325–35.

[4] Kiguchi K, Fukuda T. Position/force control of robot manipulators for geometrically unknown objects using fuzzy neural networks. IEEE Trans Ind Electron 2000;47(3):641–9.

[5] Murphy K, Norcross R, Proctor F. CAD directed robotic deburring. In: Proceedings of the second international symposium on robotics and manufacturing research, education, and applications, Albuquerque, NM; November 1988.

[6] Lu MC, Wang W-Y, Chu CY. Image-based distance and area measuring systems. IEEE Sensors J 2006;6(2):495–503.

[7] Shen TS, Huang J, Menq CH. Multiple-sensor integration for rapid and high-precision coordinate metrology. IEEE/ASME Trans Mechatron 2000;5(2):110–21.

[8] Sansoni G, Carocci M, Rodella R. Calibration and performance evaluation of a 3-D imaging sensor based on the projection of structured light. IEEE Trans Instrum Meas 2000;49(3):628–36.

[9] Sato O, Ishikawa H, Hiraki M, Takamasu K. The calibration of parallel-CMM: parallel-coordinate measuring machine, euspen 2002. Eindhoven, Holland. p. 573–76.

[10] Nguyen HG. A simple method for range finding via laser triangulation. Technical Document 2734. San Diego, CA: Naval Command, Control and Ocean Surveillance Center, RDT&E Division; January 1995.

[11] Schirripa Spagnolo G. Potentiality of 3D laser profilometry to determine the sequence of homogenous crossing lines on questioned document. Forensic Sci Int 2005.

[12] Niel A, Kölpl SH, Burgstaller M. Robotic three-dimensional measurement system for complex metal parts using structured light. PCV02(B: 190).

[13] Homh K, Ersü E, Wienand S, Lambert G. Robots as carrier for vision-sensors—chances and restrictions. In: Proceedings of the joint conference on robotics: ISR 2006, 37th international symposium on robotics and robotik 2006, 4th German conference on robotics, 15–17 May; 2006.

[14] Cinkelj J, Rejc J, Munih M. Profile measurement using robot and distance sensor. In: Proceedings of the joint conference on robotics: ISR 2006, 37th international symposium on robotics and robotik 2006, 4th German conference on robotics; 15–17 May; 2006.

[15] Teutsch C, Trostmann E, Weber M, Isenberg T. Evaluation and optimization of laser scan data. SimVis 2004; 311–22.

[16] International Standard ISO 10360-2. Geometrical product specifications (GPS)—acceptance and reverification tests for coordinate measuring machines (CMM)—Part 2: CMMs used for measuring size. Geneva, International Organization for Standardization; 2001.

[17] El-Hakim SF, Beraldin J-A, Blais F. A comparative evaluation of the performance of passive and active 3-D vision systems. In: SPIE proceedings, conference on digital photogrammetry, vol. 2646, St. Petersburg, Russia, 25–30 June 1995. p. 14–25.

[18] Curless B, Levoy M. Better optical triangulation through spacetime analysis. In: Proceedings of IEEE international conference on computer vision, Cambridge, MA, USA, 20–23 June 1995. p. 987–94.

[19] Häusler G, Kreipl S, Lampalzer R, Schielzeth A, Spellenberg B. New range sensors at the physical limit of measuring uncertainty. In: Proceedings of the EOS topical meeting on optoelectronics distance measurements and applications. Nantes, France, 8–10 July; 1997.